Journal of Materials Chemistry A

Accepted Manuscript

This article can be cited before page numbers have been issued, to do this please use: W. Wei, B. Hu, F. Jin, Z. Jing, Y. Li, A. García-Blanco, D. Stacchiola and Y. H. Hu, *J. Mater. Chem. A*, 2017, DOI: 10.1039/C7TA01768E.

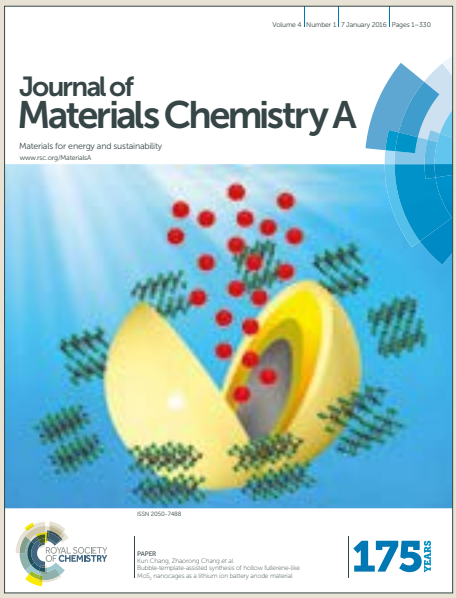

ROYAL SOCIETY OF CHEMISTRY

rsc.li/materials-a

ROYAL SOCIETY OF CHEMISTRY View Article Online
DOI: 10.1039/C7TA01768E

Journal of Materials Chemistry A

COMMUNICATION

Potassium-Chemical Synthesis of 3D Graphene from CO_2 and Its Excellent Performance for HTM-free Perovskite Solar Cells

Received 00th January 20xx,
Accepted 00th January 20xx

DOI: 10.1039/x0xx00000x

www.rsc.org/

Wei Wei,[a] Baoyun Hu,[b] Fangming Jin,[c] Zhenzi Jing,[b] Yuexiang Li,[d] Andres Alberto García Blanco,[e] Dario J. Stacchiola,[f] and Yun Hang Hu*[a]

The conversion of greenhouse gas-CO_2 to novel materials is the most promising approach to solve greenhouse gas issues. Herein, it is the firtst time to report the reaction of potassium with CO_2 to synthesize three-dimensional honeycomb-like structured graphene (3DHG). Furthermore, 3DHG exhibited excellent performance as counter electrodes for hole transport material (HTM)-free perovskite solar cells, leading to a power conversion efficiency of 10.06%. This work consitututes a new aspect of potassium chemistry for the material synthesis from a greenhouse gas and the generation of electrical energy from sunlights.

The content of CO_2, which is a major greenhouse gas causing global warming, has been increasing steadily in the atmosphere over the past centuries. Several technologies are commercially available to capture CO_2.[1-3] However, CO_2 storage is still a challenge due to its leakage from storage media and high sequestration costs.[4-6] CO_2 conversion is a promising way to solve this issue with various strategies, such as catalyzed chemical, thermochemical, electrochemical, photochemical, and photoelectrochemical.[7,8] In the recent years, Hu's group has explored the possibility of CO_2 conversion directly into novel solid materials, such as carbon nitride, lithium cyanamide, 3D cauliflower-fungus-like graphene (CFG), and crape myrtle flower-like graphene.[9-11]

Potassium, which is the second least dense metal, is of great importance for soil health, plant growth and animal nutrition. Furthermore, it plays a critical role in the fluid system and nerve functions of humans. However, to our best knowledge, no attempt has been made to exploit potassium metal for the conversion of a greenhouse gas to novel solid materials. In this communication, we demonstrate that potassium can react with CO_2 to form a new type of 3D graphene sheets. Furthermore, these graphene sheets exhibited excellent performance as a counter electrode for HTM-free perovskite solar cells with a high efficiency up to 10.06%.

In this work, the following potassium reaction is designed to convert CO_2 to graphene-structured carbon.

$$4K + 3CO_2 \rightarrow C\ (graphene) + 2K_2CO_3 \quad (1)$$

This reaction was examined by thermodynamic calculations. As shown in Fig. 1, the Gibbs free energy change is negative, indicating its thermodynamically favorable feature. Its negative enthalpy change reveals that it is exothermic. Furthermore, K_2CO_3, which are formed simultaneously with graphene, can play two important roles during the process: (1) to prevent graphite formation by isolating graphene sheets from each other and (2) to control the shape of graphene as an in-situ template, as shown in Fig. S1. This novel strategy was further confirmed experimentally as follows.

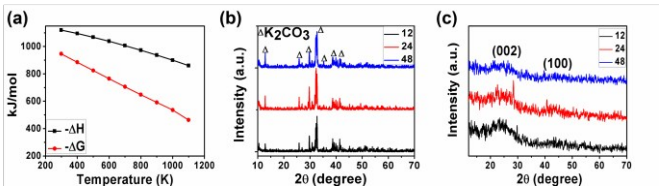

Fig. 1 Reaction between K and CO_2 to graphene and K_2CO_3: (a) changes of Gibbs free energy and enthalpy vs temperature for the reaction. (b) XRD patterns of solid products from the reaction. (c) XRD patterns of the carbon material obtained by treating the solid products with HCl.

Table 1. Graphene composition.

Samples	Elemental Analysis		EDS	
	C (%)	O (%)	C (%)	O (%)
3DHG-12	91.33	8.67	96.51	3.49
3DHG-24	92.74	7.26	96.75	3.25
3DHG-48	94.14	5.86	96.79	3.21

[a] Department of Materials Science and Engineering, Michigan Technological University, 1400 Townsend Dr. Houghton, MI, 49931, USA. Email: yunhangh@mtu.edu
[b] School of Materials Science and Engineering, Tongji University, 4800 Cao'an Road, Shanghai 201804, P. R. China.
[c] School of Environmental Science and Engineering, Shanghai Jiao Tong University, 800 Dongchuan Road, Shanghai, 200240, P. R. China.
[d] Department of Chemistry, Nanchang University, Nanchang, 330031, P. R. China.
[e] Instituto de Física Aplicada-INFAP, Departamento de Física, CONICET, UNSL (Ejercito de Los Andes 950, D5700HHW), San Luis, Argentina.
[f] Center for Functional Nanomaterials, Brookhaven National Laboratory, Upton, NY 11973, USA.
Electronic Supplementary Information (ESI) available: DOI: 10.1039/x0xx00000x

0.1mol of potassium (from Aldrich) reacted with CO_2 in a batch ceramic-tube reactor at temperature of 550 °C and an initial pressure of 50 psi for a selected time (12, 24, or 48h). The products were subjected to X-ray diffraction (XRD) evaluations. Fig. 1b shows the formation of K_2CO_3, confirming the proposed reaction. After K_2CO_3 was removed by HCl treatment, the obtained black powder was identified as carbon with oxygen functional groups by elemental analysis and energy dispersive X-ray spectrometry (EDS) (Table 1). The XRD patterns of the carbon presents a diffraction peak at 2θ =25.91°, which can be indexed to the (002) plane of graphitic structure. Another peak at 43.22° is associated with (100) plane. The broad peaks were observed due to the wrinkled and folded structure of carbon, which was further confirmed by FESEM and TEM images in the following discussion. The thickness of the primary crystal layer, which was calculated with Scherrer equation from XRD peak widths at half heights, is about 2.8 nm. Furthermore, the average interlayer space of the material is 3.44 Å, which is larger than the interlayer space of graphite. This indicates that each of the layer consists of 8 graphene sheets. Furthermore, field emission scanning electron microscope (FESEM) images show that the synthesized carbon is a three-dimensional honeycomb-like framework (Figs. 2a-2c). The thickness of each layer estimated from FESEM images is about 3.0 nm, which is consistent with that (about 2.8nm) from XRD. As a general definition, graphene material is a carbon layer consisting of 10 or less graphene sheets. Therefore, the synthesized carbon is the 3D honeycomb-structured graphene (3DHG). The 3DHG samples obtained with reaction times of 12h, 24h, and 48h are denoted as 3DHG-12, 3DHG-24, and 3DHG-48, respectively. The microstructures of 3DHG were further evaluated by transmission electron microscopy (TEM). As shown in Fig. 2d, one can see that one graphene sheet exhibits a typical wrinkled structure with corrugation and scrolling like crumped silk veil waves. Furthermore, the curved shapes were further supported by electron diffraction that shows poly-crystalline ring patterns.

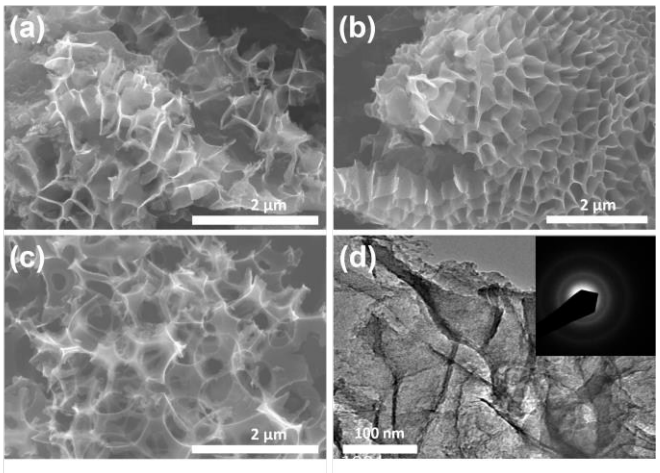

Fig. 2 Microstructures of graphene sheets: (1) FESEM images of graphene sheets obtained with reaction times of 12h (a), 24h (b), and 48h (c) and (2) TEM image of graphene sheets with the electron diffraction pattern in the inset (d).

The oxygen functional groups and defects of 3DHG were evaluated by Raman and XPS spectra. As shown in Fig. 3a, Raman spectra of 3DHG exhibit a clear G peak at 1580 cm^{-1}, providing evidence of a sp^2 bonded carbon. A strong D peak at about 1350 cm^{-1} was also observed, indicating rich defects in graphene sheets. Fig. S2 shows XPS spectra for 3DHG. The deconvolution of the C1s peak revealed four components centered at 284.6, 286.4, 288.5, and 290.5 eV, which would be associated with C-C, C-O, C=O, and O-C=O, respectively. The main component is sp^2 bonded carbon (81.4%). Furthermore, the surface area and pore structure of 3DHG were determined by N_2 adsorption. Figs. 3b-3d show a type II isotherm with a type H3 hysteresis loop, indicating that 3DHG sheets possess the mesopore structure. This was supported by the pore size distribution ranged from 5 to 90 nm (Figs. S3a-3c). The specific surface areas, which were calculated with BET model, are 946, 906, and 630 $m^2\ g^{-1}$ for 3DHG-12, 3DHG-24, and 3DHG-48, respectively. Furthermore, the sheet resistances of 3DHG films, which were also measured by four-point probe analysis, are 5.13, 4.81, and 3.97 kΩ sq^{-1} for 3DHG-12, 3DHG-24, and 3DHG-48, respectively. This indicates that 3DHG materials possess high conductivity and large surface area. In other words, they would be promising electrode materials for energy devices.

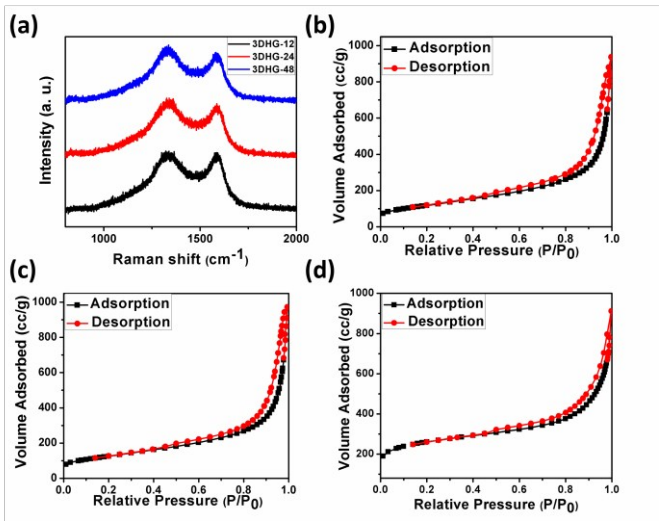

Fig. 3 Characterization of 3DHG: (1) Raman spectrum (a) and (2) Adsorption/desorption curves of 3DHG-12 (a), 3DHG-24 (b), and 3DHG-48 (c).

Solar cells have been recognized as one of the most promising technologies to relieve the global energy crisis and warming effect. Perovskite solar cells (PSCs) are attracting intensive attention due to their high power conversion efficiency (PCE), which has surpassed that of both dye-sensitized and organic solar cells and is approaching that of inorganic solar cells such as CdTe, CIGS, and even crystalline Si solar cells.[12-14] In the conventional structure of PSCs, small organic molecules (such as Spiro-OMeTAD) or organic polymers (such as P3HT, PEDOT:PSS, and PTAA) are employed as hole transport materials (HTMs), and noble Au or Ag are used as counter electrodes. The main issues that prohibit the commercial application of PSCs are their instability and high

View Article Online
DOI: 10.1039/C7TA01768E

fabrication cost. A simple way to cut down fabrication cost is the development of HTM free perovskite solar cells due to the ambipolar charge transfer property of the methylammonium lead iodide perovskite.[15-17] Etgar et al. fabricated the first heterojunction FTO/TiO_2/$CH_3NH_3PbI_3$/Au cell, achieving initial PCE of 5.5%.[18] They improved the PCE to 8.1% using a 300 nm mesoporous TiO_2 film and tuning the perovskite layer[19] and then to 10.85% using the two-step deposition technique.[20] The elimination of unstable organic HTM can also remarkably increase the stability of PSCs. Furthermore, noble metal counter electrodes can be replaced by earth abundant, low-cost, and chemical stable carbon materials.[21-26] Those have stimulated us to explore 3DHG as counter electrodes for HTM-free PSCs. To fabricate the device of HTM-free perovskite solar cell, 3DHG was coated on the $CH_3NH_3PbI_3$ layer as a counter electrode with doctor-blade method. To improve the interface, the 3DHG was introduced into the solution of perovskite precursors, followed by the in-situ synthesis of the perovskite layer. As a result, a transition layer, in which part of $CH_3NH_3PbI_3$ perovskite molecules were highly dispersed on 3DHG, was formed between the perovskite layer and the 3DHG counter electrode. Fig. 4a shows the configuration (HTM-free TiO_2/$CH_3NH_3PbI_3$/3DHG//3DHG) of fabricated perovskite solar cells, in which the HTM layer was eliminated and the novel metal electrode was replaced by 3DHG. Fig. 4b shows the current density (I)-voltage (V) characteristics of HTM-free 3DHG-based PSCs. The short-circuit photo-current (I_{sc}), open-circuit voltage (V_{oc}), fill factor (ff), and power conversion efficiency (η) for 3DHG-12-based cell are 17.79 mA cm^{-2}, 0.87 V, 0.50, and 7.71%, respectively. When the synthesizing time increased to 48h, power conversion efficiency (η) increased to 10.06% with enhanced I_{sc} (18.11 mA cm^{-2}), V_{oc} (0.89 V), and ff (0.63). This happened probably because the increase in the synthesis time of 3DHG enhanced its electrical conductivity. It is well-known that some perovskite solar cells suffer an issue that a photocurrent hysteresis occurs at certain voltage scanning rate and scan direction. This issue is usually caused by either charge traps in low quality perovskite films or ferroelectric properties of the perovskite materials and/or the electromigration of ion in perovskites.[27-29] However, such a hysteresis was not observed for the perovskite solar cell with the 3DHG counter electrode (Fig. 5a). The excellent performance of the 3DHG-based perovskite solar cells was further supported by the incident-photon-to-current conversion efficiency (IPCE). As shown in Fig. 5b, one can see the IPCE curve with a strong spectral response in the range from 350 to 750 nm. The integrated current from the IPCE curve is very close to the I_{sc} obtained from the I-V curve. EIS measurement was carried out in the frequency range of 1 Hz to 1 MHz with 10 mV AC amplitude under dark condition. Fig. 5c depicts the Nyquist plot of solar cell with 3DHG CEs at a forward bias of 900 mV. The first semi-circle in the high frequency region is assigned to the charge exchange process at the perovskite/CE interface, while the one at low frequencies represents the TiO_2/perovskite interface. The negative capacitance appears in the low frequency region corresponding to an additional recombination pathway at high forward bias at one of the interfaces. 3DHG-48 based PCS shows the smallest radius of the semicircle in the high frequency (Fig. S5b), which indicates the lowest charge transfer resistance at the $CH_3NH_3PbI_3$/carbon interface.[30,31] Capacitance-voltage (Cap-V) analysis was further conducted to evaluate depletion region in the cell. The corresponding Mott-Schottky curves are displayed in Fig. 5d. According to the junction capacitance, the built-in potential was extrapolated using the intercept of the linear regime with the x-axis of the Mott-Schottky plot and equal to 0.98V, which is consistent with the V_{oc} of the photovoltaic device. The presence of a built-in field can efficiently force the separation of photogenerated carriers and suppress the back reaction of electrons from the TiO_2 film to the $CH_3NH_3PbI_3$ layer. Finally, the excellent preparation-reproducibility of cells was demonstrated by the histogram of efficiencies for 10 cells (Fig. S4).

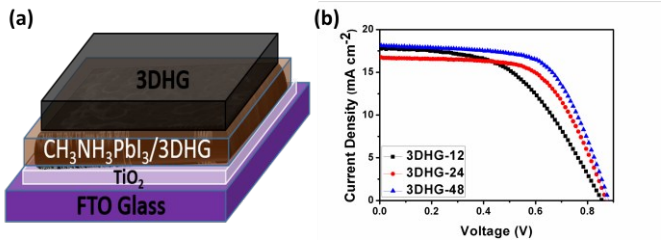

Fig. 4 HTM-free perovskite photovoltaic performance: (a) cell configuration of 3DHG-based perovskite solar cell and (b) I–V curves of PSCs with 3DHG counter electrodes.

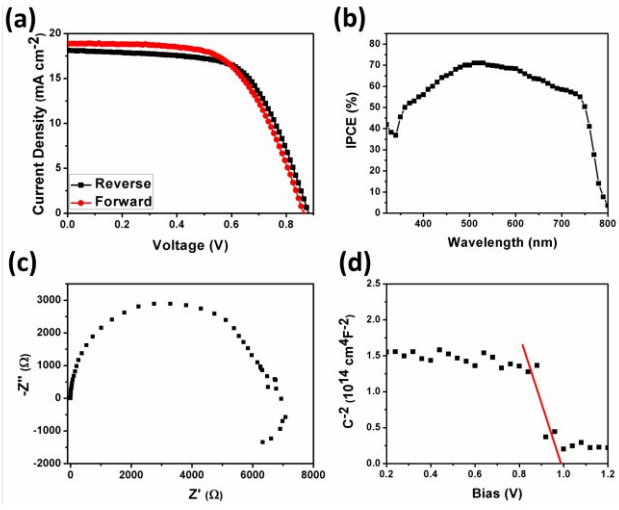

Fig. 5 Characterization of a HTM-free PSC with 3DHG-48 counter electrode: (a) I–V curves, (b) IPCE curve, (c) Nyquist plot, and (d) Mott–Schottky plot.

Table 2. Photovoltaic performance of PSCs with 3DHG CE.

CEs	I_{sc} (mA cm-2)	V_{oc} (V)	ff	Efficiency (%)
3DHG-12	17.79	0.87	0.50	7.71
3DHG-24	16.75	0.87	0.62	9.01
3DHG-48	18.11	0.89	0.63	10.06

Table 3. Photovoltaic performance of PSCs with 3DHG-48 as CE.

CEs	I_{sc} (mA cm^{-2})	V_{oc} (V)	ff	Efficiency (%)
Reverse	18.11	0.89	0.63	10.06
Forward	18.86	0.86	0.61	9.84

Conclusions

In summary, a reaction between K and CO_2 was invented to synthesize 3D honeycomb-structured graphene, which possesses high conductivity. Furthermore, the 3D honeycomb-structured graphene exhibited excellent performance as counter electrodes for HTM-free perovskite solar cells, leading to the high power conversion efficiency of 10.06%. This novel 3D graphene can also be applied for batteries, fuel cells, and supercapacitors, which will be reported in our future papers. Therefore, this work provided a new aspect of potassium chemistry for CO_2 conversion and created excellent electrode materials for energy devices.

Acknowledgements

This work was supported by the ACS Petroleum Research Fund (PRF-51799-ND10). WW and YHH thank Charles and Carroll McArthur for their great support.

Notes and references

1 A. B. Rao and E. S. Rubin, *Environ. Sci. Technol.,* 2002, **36**, 4467-4475.
2 D. Camper, J. E. Bara, D. L. Gin, and R. D. Noble, *Ind. Eng. Chem. Res.*, 2008, **47**, 8496-8498.
3 J. D. Figueroa, T. Fout, S. Plasynski, H. McIlvried, R. D. Srivastava, *Int. J. Greenh Gas Con.*, 2008, **2**, 9-20.
4 L. Hammarström and S. Hammes-Schiffer, *Acc. Chem. Res.,* 2009, **42**, 1859–1860.
5 A. Kumar, M. Noh, G. A. Pope, K. Sepehrnoori, S. Bryant, and L. W. Lake, *SPE J.*, 2005, **10**, 336-348.
6 M. A. Barrufet, K. S. El-Sayed, S. M. Tantawy, and G. A. Iglesias-Silva, *J. Chem. Eng. Data*, 1996, **41**, 436-439.
7 Y. H. Hu and E. Ruckenstein, *Adv. Catal.,* 2004, **48**, 297-345.
8 A. Goeppert, M. Czaun, J. P. Jones, G. K. Surya Prakash, and G. A. Olah, *Chem. Soc. Rev.*, 2014, **43**, 7995–8048.
9 Y. H. Hu and Y. Huo, *J. Phys. Chem. A*, 2011, **115**, 11678-11681.
10 W. Wei, K. Sun, and Y. H. Hu, *J. Mater. Chem. A,* 2014, **2**, 16842-16846.
11 W. Wei, K. Sun, and Y. H. Hu, *J. Mater. Chem. A,* 2016, **4**, 12054-12057.
12 Best Research Cell Efficiencies, http://www.nrel.gov/ncpv/images/efficiency_chart.jpg (accessed September 2016).
13 M. He, X. Pang, X. Liu, B. Jiang, Y. He, H. Snaith, and Z. Lin, *Angew. Chem. Int. Ed.,* 2016, **55**, 4280-4284.
14 M. He, D. Zhang, M. Wang, C. Lin, and Z. Lin, *J. Mater. Chem. A*, 2014, **2**, 5994-6003.
15 S. D. Stranks, G. E. Eperon, G. Grancini, C. Menelaou, M. J. Alcocer, T. Leijtens, L. M. Herz, A. Petrozza, and H. J. Snaith, *Science*, 2013, **342**, 341–344.
16 G. Xing, N. Mathews, S. Sun, S. S. Lim, Y. M. Lam, M. Grätzel, S. Mhaisalkar, and T. C. Sum, *Science*, 2013, **342**, 344–347.
17 Z. Wei, K. Yan, H. Chen, Y. Yi, T. Zhang, X. Long, J. Li, L. Zhang, J. Wang, and S. Yang, *Energy Environ. Sci.*, 2014, **7**, 3326–3333.
18 L. Etgar, P. Gao, Z. Xue, Q. Peng, A. K. Chandiran, B. Liu, M. K. Nazeeruddin, and M. Grätzel, *J. Am. Chem. Soc.*, 2012, **134**, 17396–17399.
19 W. A. Laban, and L. Etgar, *Energy Environ. Sci.*, 2013, **6**, 3249–3253.
20 S, Aharon, S. Gamliel, B. Cohen, and L. Etgar, *Phys. Chem. Chem. Phys.*, 2014, **16**, 10512-10518.
21 K. Fu, Q. Zhou, Y. Chen, J. Lu, and S. Yang, *J. Opt.*, 2015, **17**, 105904-105910.
22 Y. Li, L. Xu, H. Liu, and Y. Li, *Chem. Soc. Rev.*, 2014, **43**, 2572–2586.
23 C. Huang, S. Zhang, H. Liu, Y. Li, G. Cui, and Y. Li, *Nano. Energy*, 2015, **11**, 481–489.
24 J. Shi, Y. Luo, H. Wei, J. Luo, J. Dong, S. Lv, J. Xiao, Y. Xu, L. Zhu, X. Xu, H. Wu, D. Li, and Q. Meng, *ACS Appl. Mater. Interfaces,* 2014, **6**, 9711-9718.
25 Z. Ku, Y. Rong, M. Xu, T. Liu, and H. Han, *Sci. Rep.*, 2013, **3**, 3132-3136.
26 K. Yan, Z. Wei, J. Li, H. Chen, Y. Yi, X. Zheng, X. Long, Z. Wang, J. Wang, J. Xu and S. Yang, *Small*, 2015, **11**, 2269–2274.
27 H. J. Snaith, A. Abate, J. M. Ball, G. E. Eperon, T. Leijtens, N. K. Noel, S. D. Stranks, J. T. Wang, K. Wojciechowski, and W. Zhang, *J. Phys. Chem. Lett.*, 2014, **5**, 1511-1515.
28 H-W. Chen, N. Sakai, M. Ikegami, and T. Miyasaka, *J. Phys. Chem. Lett.*, 2015, **6**, 164-169.
29 B. Chen, M. Yang, S. Priya, and K. Zhu, *J. Phys. Chem. Lett.*, 2016, **7**, 905-917.
30 M. Xu, Y. Rong, Z. Ku, A. Mei, T. Liu, L. Zhang, X. Li, and H. Han, *J. Mater. Chem. A*, 2014, **2**, 8607-8611.
31 F. Zhang, X. Yang, H. Wang, M. Cheng, J. Zhao, and L. Sun, *ACS Appl. Mater. Interfaces*, 2014, **6**, 16140-16146.

View Article Online
DOI: 10.1039/C7TA01768E

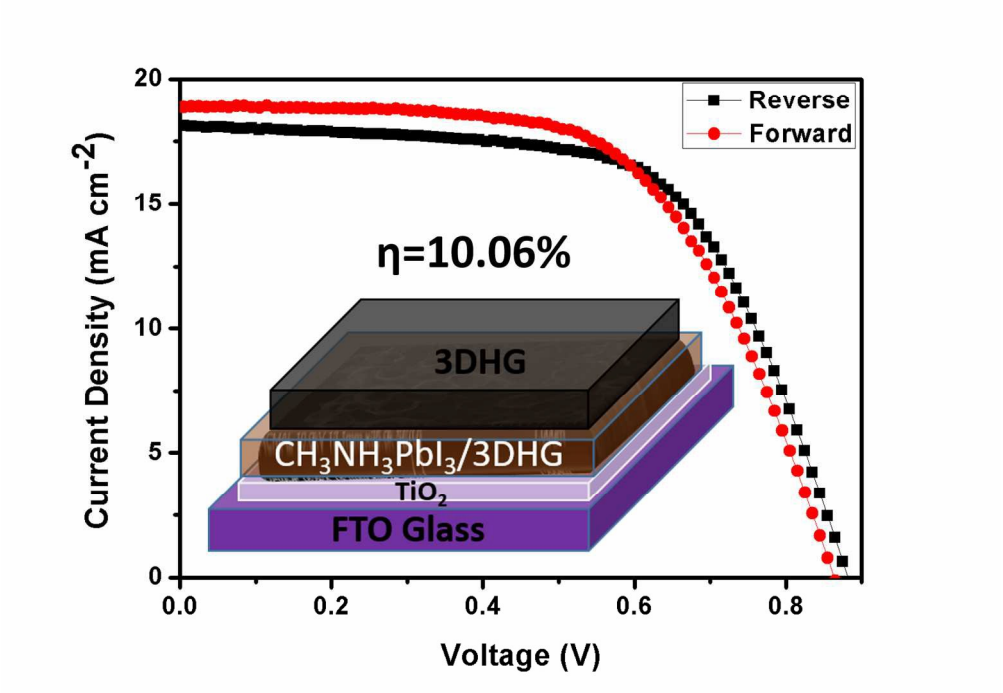

503x350mm (96 x 96 DPI)